A New Phase Boundary in $(Bi_{1/2}Na_{1/2})TiO_3$–$BaTiO_3$ Revealed via a Novel Method of Electron Diffraction Analysis

Cheng Ma, Hanzheng Guo, and Xiaoli Tan**

A new phase boundary is revealed in $(1–x)(Bi_{1/2}Na_{1/2})TiO_3$–$xBaTiO_3$, the most extensively studied lead-free piezoelectric solid solution. This discovery results from a novel method of electron diffraction analysis, which allows the precise determination of oxygen octahedra tilting in multi-domain perovskite ferroelectrics. The study using this method supports the recently proposed *Cc* symmetry for pure $(Bi_{1/2}Na_{1/2})TiO_3$, and, more importantly, indicates the crystal structure evolves into the *R3c* symmetry with the addition of $BaTiO_3$, forming a *Cc*/*R3c* phase boundary at $x = 3–4\%$. In the poling field E_{pol} versus composition *x* phase diagram for polycrystalline ceramics, this phase boundary exists with E_{pol} below 5.5 kV mm^{-1}; the *Cc* phase is transformed to the *R3c* phase during poling at higher fields. The results reported here provide the microstructural origin for the previously unexplained strain behavior and clarify the low-$BaTiO_3$-content phase relationship in this popular lead-free piezoelectric system.

1. Introduction

Ferroelectric materials with strong piezoelectricity are critical in numerous important applications including energy harvesting,[1,2] non-volatile memories,[3] and medical imaging.[1,2,4] Knowledge of the subtle crystal structure distortions in ferroelectrics is key to understanding and optimizing the properties; the morphotropic phase boundary (MPB), where piezoelectricity peaks due to the coexistence of multiple ferroelectric phases,[1,4] cannot be thoroughly characterized without precise structural analysis. Recently, the investigation of MPBs becomes even more compelling due to the increasingly urgent global demand for high-performance environmentally friendly lead-free piezoelectrics.[4–7] In particular, several fundamental issues regarding the crystal structures and phase relationships of the most extensively studied piezoelectric system, $(1–x)(Bi_{1/2}Na_{1/2})TiO_3$–$xBaTiO_3$,[4] are still not well understood.

Over years, the base compound $(Bi_{1/2}Na_{1/2})TiO_3$, whose structures and phase relationships are largely inherited by the optimal compositions $x \approx 7\%$,[4,8–12] is believed to crystallize in the *R3c* symmetry with $a^-a^-a^-$ oxygen octahedra tilting.[13] The polar axis, [111] direction, coincides with the octahedra tilting axis.[13] With increasing *x*, the structure evolves into the *P4bm* symmetry at $x \approx 6\%$ and then *P4mm* at $x \approx 11\%$.[9–12] Recently, the space group of $(Bi_{1/2}Na_{1/2})TiO_3$ is found to be *Cc* instead of *R3c*.[14–16] This *Cc* symmetry does not deviate dramatically from the *R3c* symmetry in terms of the unit cell dimensions; the pseudocubic unit cell of the *Cc* symmetry displays lattice constants of $a = b = 3.887$ Å, $c = 3.882$ Å, $\alpha = \beta = 89.944°$, $\gamma = 89.646°$, while that of the *R3c* symmetry exhibits the lattice constants of $a = b = c = 3.885$ Å, $\alpha = \beta = \gamma = 89.83°$.[14] Nevertheless, the octahedra tilting clearly differs. Unlike the *R3c* symmetry showing an $a^-a^-a^-$ tilting around the [111] axis, the *Cc* symmetry exhibits $a^-a^-c^-$ octahedra tilting, and the tilting axis, coinciding with the polar axis, is the [*uuv*] direction.[14–16] The aforementioned structural update brings up one question immediately: do all the solid solution compositions with $x < 6\%$ exhibit the *Cc* symmetry like $(Bi_{1/2}Na_{1/2})TiO_3$? The answer to this question could possibly lead to the discovery of an MPB that has been overlooked for long in this most extensively studied piezoelectric system.

Despite the importance of pursuing the answer to this question, several technical difficulties exist. The crystal structure of perovskite ferroelectrics often involves both atomic displacement and oxygen octahedra tilting.[17] While the former may be conveniently revealed through X-ray/neutron diffraction, the latter, which happens to be critical in distinguishing the *R3c* and *Cc* symmetries as mentioned above, can hardly be unraveled in a straightforward way.[18] The superlattice diffractions characterizing different octahedra tilting are usually too weak to be examined properly.[18] Besides, in most cases, tilting occurs over a short coherence length, while X-ray/neutron diffraction collects average structural information over much larger length scales.[18]

It has been acknowledged that transmission electron microscopy (TEM), a very convenient tool for studying the subtle crystal structures of perovskite ferroelectrics,[18–26] is more effective in solving the octahedra tilting.[18–23] While convergent beam electron diffraction in TEM has also been employed for

Dr. C. Ma, H. Guo, Prof. X. Tan
Department of Materials Science and Engineering
Iowa State University
Ames, IA 50011, USA
E-mail: macheng02@gmail.com; xtan@iastate.edu

DOI: 10.1002/adfm.201300640

such an analysis,[20–23] the attempt to study octahedra tilting using selected area electron diffraction was made in early 1990s,[19] and a commonly used analysis method for this diffraction technique was proposed and comprehensively summarized by Reaney and co-workers years ago.[18,27] Unlike X-ray/neutron diffraction, this method relies on the axis about which the octahedra tilting occurs, instead of any specific superlattice diffractions. Thus it is more straightforward. However, this method is applicable only for the study of one single domain, and also involves significant specimen tilting. Unfortunately, ferroelectric domains are often too small to be studied individually using selected area electron diffraction,[28–31] and in many cases the required specimen tilting cannot be realized in a standard double-tilt holder.[18,27] Hence the determination of octahedra tilting with electron diffraction is still challenging.

In this study, we propose a more practical method to analyze octahedra tilting under TEM; it works in the multi-domain state, and the specimen tilting between different zone axes is much simpler, or even unnecessary. Using this method, we discovered a new phase boundary in $(Bi_{1/2}Na_{1/2})TiO_3$–$BaTiO_3$; the *Cc* symmetry in $(Bi_{1/2}Na_{1/2})TiO_3$ was found to evolve into the *R3c* symmetry with increasing $BaTiO_3$ content. This discovery elucidates the previously unexplained strain behaviors[32] and clarifies the low-$BaTiO_3$-content phase relationship in this intriguing system. Beyond $(Bi_{1/2}Na_{1/2})TiO_3$–$BaTiO_3$, the methodology proposed here is generally applicable to the distinction of different symmetries in other perovskite ferroelectrics involving subtle oxygen octahedra tilting.

Table 1. {010} domain configurations for the *R3c* and *Cc* symmetries.

		{010} domain walls		
		(010)	(100)	(001)
R3c ($a^-a^-a^-$)	$\boldsymbol{P}_1$, $\boldsymbol{P}_2$[a]	[111], $[\bar{1}\,\bar{1}\,\bar{1}]$	[111], $[1\,\bar{1}\,\bar{1}]$	[111], $[\bar{1}\,\bar{1}\,1]$
	$\cos\theta$[b]	-1/3	-1/3	-1/3
	$\boldsymbol{P}_1 \times \boldsymbol{P}_2$[c]	$[\bar{1}01]$	$[01\bar{1}]$	$[1\bar{1}0]$
	Domain configuration probability[d]	100%		
	Extinction probability[e]	50%		
Cc ($a^-a^-c^-$)	$\boldsymbol{P}_1$, $\boldsymbol{P}_2$[a]	$[uuv]$, $[\bar{u}u\bar{v}]$	$[uuv]$, $[u\bar{u}\bar{v}]$	$[uuv]$, $[\bar{u}\bar{u}v]$
	$\cos\theta$[b]	$-v^2/(v^2+2u^2)$	$-v^2/(v^2+2u^2)$	$(v^2-2u^2)/(v^2+2u^2)$
	$\boldsymbol{P}_1 \times \boldsymbol{P}_2$[c]	$[\bar{v}0\,u]$	$[0v\bar{u}]$	$[1\bar{1}0]$
	Domain configuration probability[d]	66.7%		33.3%
	Extinction probability[e]	16.7%		

[a] $\boldsymbol{P}_1$ and $\boldsymbol{P}_2$ denote the polar axes (parallel with the oxygen octahedra tilting axes for both symmetries) of the two adjacent domains, respectively; [b] θ denotes the angle between $\boldsymbol{P}_1$ and $\boldsymbol{P}_2$; [c] Listed here are the low-index directions parallel to $\boldsymbol{P}_1 \times \boldsymbol{P}_2$, rather than the actual result of the cross product; [d] Listed here is the probability that each {010} domain configuration occurs. Note that the domain configuration differs by $\cos\theta$, rather than the {010} plane that the domain wall lies in; [e] Listed here is the probability of 1/2{*ooo*} spots being absent along a randomly selected <101> zone axis within the {010} domain wall plane.

2. Methodology

A detailed analysis of domain configurations is necessary before the *R3c* and *Cc* symmetries, or practically the $a^-a^-a^-$ and $a^-a^-c^-$ octahedra tilting systems, can be distinguished through multi-domain electron diffraction. While the domain wall could possibly lie along several different planes, only the {010} domains, which have been observed to show a high number density in the composition of interest,[16,30] need to be studied in order to differentiate between the two symmetries. **Table 1** lists the possible {010} domain configurations of the *R3c* and *Cc* symmetries. The polar axes (coincide with octahedra tilting axes for both symmetries) of the two adjacent domains separated by a {010} domain wall must be non-parallel crystallographically equivalent directions that form the same angle with the domain wall plane and also satisfy the domain-wall charge-neutral condition. In this sense, once the polar axis of one domain (denoted as $\boldsymbol{P}_1$) and the domain wall plane are known, the polar axis of the other domain (denoted as $\boldsymbol{P}_2$) becomes unique and can thus be easily determined. In the case of {010} planes, the domain wall can possibly lie within three planes: (010), (100), or (001). Therefore, if $\boldsymbol{P}_1$ is fixed, $\boldsymbol{P}_2$ has three possibilities, each of which corresponds to a {010} plane. In Table 1, $\boldsymbol{P}_1$ is fixed as [111] and $[uuv]$ for the *R3c* and *Cc* symmetries, respectively, and the possible $\boldsymbol{P}_2$ are listed. Although all of the domain wall planes, as well as the involved polar axes, are crystallographically equivalent for each symmetry, different domain configurations still emerge: the angle between $\boldsymbol{P}_1$ and $\boldsymbol{P}_2$ (denoted as θ) could differ. As shown in Table 1, while the *R3c* symmetry exhibits the same θ in all three possibilities (indicating it has only one {010} domain configuration), the *Cc* symmetry shows two different θ values. The (010) and (100) domains yield $\cos\theta = -v^2/(v^2+2u^2)$, but the (001) domains $\cos\theta = (v^2-2u^2)/(v^2+2u^2)$. Therefore, the *Cc* symmetry has two different {010} domain configurations.

The *R3c* and *Cc* symmetries are discerned via the different diffraction behaviors of these {010} domain configurations. The antiphase oxygen octahedra tilting in both symmetries yields 1/2{*ooo*} (*o* represents odd Miller indices) diffractions.[17,18] The diffraction intensity formula suggests these 1/2{*ooo*} spots become invisible when the octahedra tilting axis happens to be perpendicular to the <101> zone axis selected for electron diffraction analysis.[17,18] Consequently, if an ensemble of {010} domains are studied, the 1/2{*ooo*} spots are absent only when the octahedra tilting axes in both domain variants ($\boldsymbol{P}_1$ and $\boldsymbol{P}_2$ in Table 1) are simultaneously perpendicular to the observation zone axis. Note that any two non-parallel vectors are simultaneously perpendicular to one direction only: their cross product. Therefore, if $\boldsymbol{P}_1 \times \boldsymbol{P}_2$ coincides with one <101> axis, this and only this <101> axis, which also happens to be one of the two <101> axes within the {010} domain wall plane in all cases (Table 1), does not show 1/2{*ooo*} spots; if not, any <101> axis, including the two within the domain wall plane, exhibits 1/2{*ooo*} spots. As shown in Table 1, the *R3c* symmetry belongs to the former case no matter which {010} plane the domain wall lies on. This domain configuration is schematically illustrated in **Figure 1**a. Between the two <101> axes within the

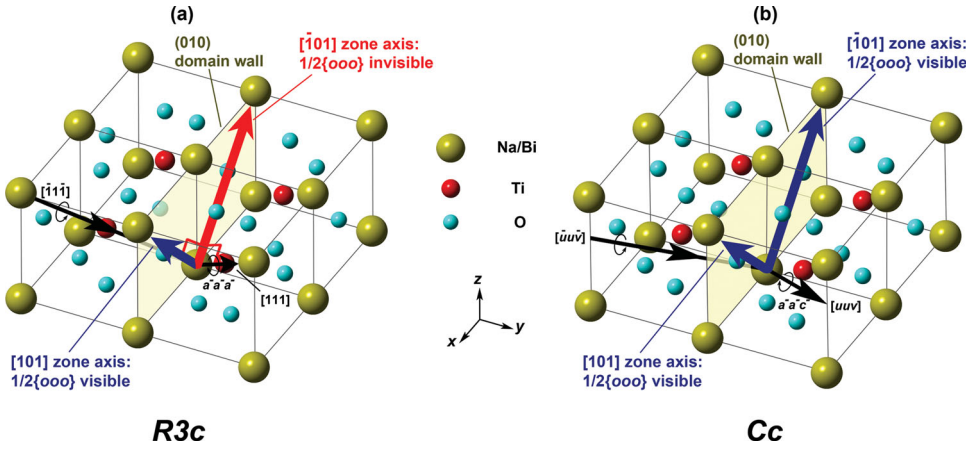

Figure 1. The {010} domain configurations that differentiate between the *R3c* ($a^-a^-a^-$) and *Cc* ($a^-a^-c^-$) symmetries.

domain wall (yellow shade), [$\bar{1}$01] (red arrow) is perpendicular to the octahedra tilting axes in both domains (black arrows), but [101] (blue arrow) is not. Therefore, 1/2{*ooo*} spots are absent if the diffraction pattern is formed along [$\bar{1}$01], but present if along [101]. Unlike *R3c*, the {010} domains in the *Cc* symmetry have two possible configurations (Table 1). The one with $\cos\theta = -v^2/(v^2 + 2u^2)$, whose $\boldsymbol{P}_1 \times \boldsymbol{P}_2$ is not parallel with any <101> zone axis, is illustrated in Figure 1b. Clearly neither <101> zone axis (blue arrows) within the domain wall (yellow shade) is perpendicular to octahedra tilting axes (black arrows), so both of them display 1/2{*ooo*} spots. In contrast, the configuration with $\cos\theta = (v^2 - 2u^2)/(v^2 + 2u^2)$ shows a $\boldsymbol{P}_1 \times \boldsymbol{P}_2$ parallel with a <101> zone axis (Table 1), and forbids 1/2{*ooo*} spots along one of the two <101> axes within the domain wall like *R3c*. Therefore, it cannot be used to distinguish between the two symmetries. Since the probability for each of the three {010} planes being the domain wall should be equal, this configuration only has a 33.3% chance of occurring, and the one that differentiates the *Cc* from *R3c* symmetry has a 100% – 33.3% = 66.7% chance (Table 1).

Based on these analyses, the operation procedure under TEM is as follows: 1) with the specimen tilting close to zero, find a grain along the <001> zone axis with an ensemble of domains exhibiting edge-on {010} domain walls; 2) while maintaining the {010} domain walls edge-on, tilt the specimen to the two adjacent <101> axes. The edge-on condition ensures that these two <101> axes are the ones within the domain wall plane. If both axes show 1/2{*ooo*} spots, the symmetry is *Cc*. If the absence of 1/2{*ooo*} spots along one of the two <101> zone axes is repeatedly observed in many grains without any exception, the symmetry is *R3c*.

Alternatively, if the number of grains studied is reasonably large, only one randomly selected <101> axis within the {010} domain wall needs to be examined. For *R3c*, since the only {010} domain configuration forbids 1/2{*ooo*} diffraction along one of the two <101> zone axes (Table 1, Figure 1a), these superlattice spots have a 50% chance of being absent (referred to as the "extinction probability" below). For *Cc*, the domain configuration with the same diffraction behavior has a 33.3% chance of occurring (Table 1), so 1/2{*ooo*} spots have a 33.3% × 50% = 16.7% chance of being absent. As a result, the symmetry can be inferred from the number of grains that are observed to show diffraction patterns without 1/2{*ooo*} spots.

While both the two-pole complete approach and the one-pole statistical approach described above are developed from the same methodology, their applicability varies. The advantage of the two-pole approach lies in its capability of revealing the symmetry of the individual grain. Nevertheless, the ±45° tilting it requires cannot be performed on a TEM with high-resolution polepieces, which typically has a tilting limit of ±35°. Even for a TEM with conventional polepieces, the ±45° tilting would be more convenient only along or close to the primary tilting direction of the specimen holder. Considering this practical issue, a tilt-rotate TEM holder would be a better choice than a regular double-tilt one. In contrast, the alternative one-pole approach is virtually not restrained by the instrument tilting limit and is much easier in TEM operation, if the two symmetries to be distinguished show apparently different diffraction behaviors, for example, 50% versus 16.7% extinction probability, as shown in Table 1. As will be demonstrated below in $x = 3.5\%$, the number of grains that need to be studied to differentiate between such two extinction probabilities does not have to be unrealistically large. The drawback of the one-pole approach is that it does not directly determine the symmetry of individual grains and is particularly less indicative in discerning two symmetries with similar extinction probabilities.

It should be noted that our method is applicable for multi-domain study, and the zone axes that need to be examined could be as few as one. In contrast, the commonly used method[18,27] is suitable for single-domain study only, which could hardly be performed in many systems due to the absence of sufficiently large domains. Besides, it requires complicated specimen tilting among four zone axes (Supporting Information, Table S1, Figure S1). The key to the significantly lowered operation difficulty of our method lies in the use of domain wall edge-on conditions, which allows the exclusive selection of

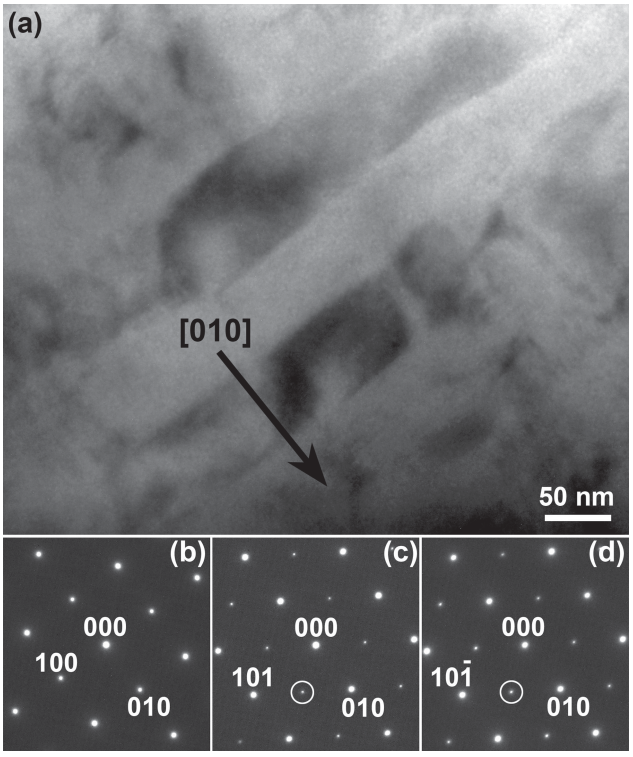

Figure 2. TEM results of $(Bi_{1/2}Na_{1/2})TiO_3$. a) Bright-field image of an ensemble of edge-on {010} domains along the [001] zone axis. Selected area diffraction patterns of these domains along the b) [001], c) $[\bar{1}01]$, and d) [101] zone axes are also displayed with 1/2{*ooo*} spots highlighted by bright circles. The orientation of these diffraction patterns has been adjusted to compensate the image-to-diffraction rotation.

specific zone axes among the many crystallographically equivalent ones. Therefore, even though the multi-domain state is more complicated than the single-domain state, its octahedra tilting can be determined with much simpler TEM operations. The same idea can also be used to simplify the distinction of other symmetries in perovskite ferroelectrics. Despite these advantages, it must also be pointed out that this technique has its limitations. For example, it is not applicable for overlapping regions with edge-on and non-edge-on domains, ferroelectrics with domain morphologies sensitive to electron beam irradiation, compounds subject to changes during TEM specimen preparation, and so forth.

3. TEM Results

Using the method described above, two compositions of $(1–x)(Bi_{1/2}Na_{1/2})TiO_3–xBaTiO_3$, x = 0 and 3.5%, were studied to clarify the phase relationship for x <6%. **Figure 2**a displays the bright-field image of a representative grain in pure $(Bi_{1/2}Na_{1/2})TiO_3$ along the [001] zone axis, which shows an ensemble of edge-on domains. A comparison between this bright-field image and the diffraction pattern recorded along the same zone axis (Figure 2b) shows that these edge-on domain walls lie on planes close to (010). With these domain walls remaining

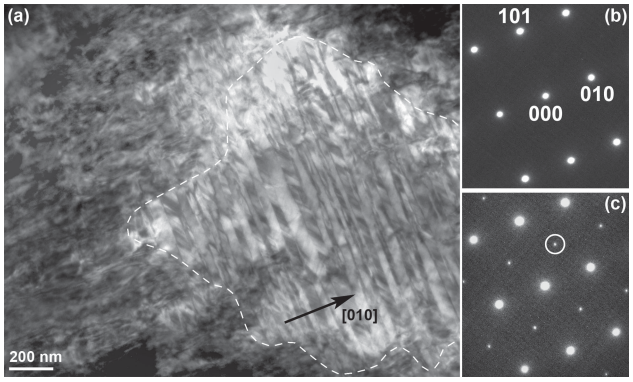

Figure 3. TEM results of $(1–x)(Bi_{1/2}Na_{1/2})TiO_3–xBaTiO_3$ with x = 3.5%. a) Bright-field image of a grain along the $[\bar{1}01]$ zone axis. The region showing edge-on domains are delineated with dashed lines. The selected area diffraction patterns of the b) edge-on and c) non-edge-on domains along the same orientation are also displayed. One of the 1/2{*ooo*} spots in (c) is highlighted by the bright circle. The orientation of these diffraction patterns has been adjusted to compensate the image-to-diffraction rotation.

edge-on, the grain was tilted to its $[\bar{1}01]$ and [101] axes. Due to the larger specimen thickness that the electron beam needs to penetrate at higher specimen tilting angles, the contrast of these edge-on domains became obscured in the two <101> axes, but still distinguishable. Despite this, 1/2{*ooo*} spots were observed along both <101> axes within the (010) domain wall plane (Figure 2c,d). According to Table 1 and Figure 1, such a diffraction behavior cannot occur for the *R3c* symmetry, but can only be yielded by the *Cc* {010} domain configuration with $\cos\theta = -v^2/(v^2 + 2u^2)$. Therefore, this TEM study, which was performed with the method we proposed above, supports the recent results about the *Cc* symmetry for pure $(Bi_{1/2}Na_{1/2})TiO_3$.[14–16]

Figure 3 shows the TEM results of a grain along its $[\bar{1}01]$ zone axis in the $(1–x)(Bi_{1/2}Na_{1/2})TiO_3–xBaTiO_3$ ceramic with x = 3.5%. A portion of the grain (delineated by dashed lines in Figure 3a) contains domains with edge-on walls, which lie on the (010) plane as suggested by the comparison between the bright-field image and the selected area electron diffraction pattern taken from the same region (Figure 3b). While the non-edge-on domains showed 1/2{*ooo*} spots (Figure 3c) as expected,[17,18] no 1/2{*ooo*} spots were observed in the edge-on domains (Figure 3b). Among the seven grains studied in this specimen, four showed the same results. Should the specimen be phase-pure with the *Cc* symmetry, the probability of 1/2{*ooo*} spots being absent in a single observation is 16.7% (Table 1), and thus the probability of observing this in 4 out of 7 grains is $(16.7\%)^4 \times (1 - 16.7\%)^3 \times C(7,4) = 1.57\%$, which is extremely unlikely. A similar study was performed on two other x = 3.5% specimens, and the results corroborated each other: around half of the grains studied did not display 1/2{*ooo*} spots along the $[\bar{1}01]$ zone axis. Therefore, it is safe to conclude that the *R3c* phase is present in the composition x = 3.5%, although the coexistence of the *Cc* phase should not be excluded.

The TEM results, along with previous studies,[14–16] clearly suggest a composition-induced *Cc*-to-*R3c* phase transition occurs somewhere at x < 6%. Recent measurements on

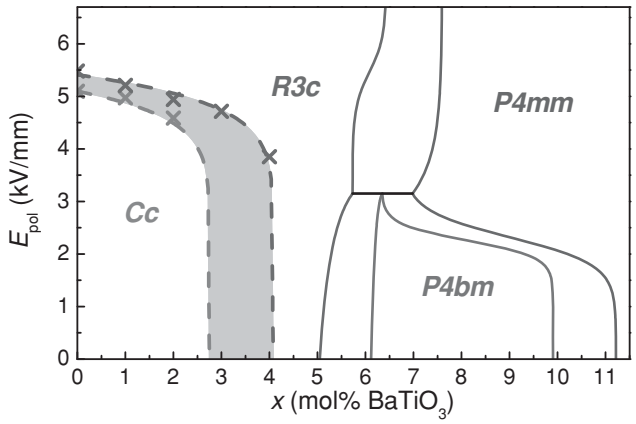

Figure 4. The poling field E_{pol} vs. composition x phase diagram for polycrystalline $(1–x)(Bi_{1/2}Na_{1/2})TiO_3–xBaTiO_3$ ceramics. The *Cc*/*R3c* phase boundary (green band) is revealed in this study, with critical fields (crosses) obtained from the strain curves.[32] Other phase boundaries are determined in our previous study.[12]

electric-field-induced strains indicate that certain low-$BaTiO_3$-content compositions experience an irreversible phase transition under poling fields, while the structural change during this transition is unknown.[32] If the critical fields of this transition are plotted in the poling field E_{pol} versus composition x phase diagram for polycrystalline ceramics,[12] a phase boundary running through x = 3–4% at zero poling field forms (green band in **Figure 4**). According to our TEM results, this phase boundary is very likely to be the *Cc*/*R3c* phase boundary. This scenario is also supported by the discontinuity at x = 3–4% in the remanent volume strain V_{rem} versus composition x plot (Supporting Information, Figure S2),[32] and the recently observed *R3c* symmetry in the 7 kV mm^{-1}-poled $(Bi_{1/2}Na_{1/2})TiO_3$ ceramic.[33] The new *Cc*/*R3c* phase boundary reported here indicates the previously unexplained electric-field-induced phase transition[32] is a *Cc*-to-*R3c* structural transition. Despite these new insights regarding the phase relationships, the results presented here are consistent with previous TEM studies on similar compositions.[34,35]

Finally, it should be made clear that TEM, as a tool for local structure analysis, cannot conclusively determine the overall phase structure of a polycrystalline ceramic specimen. The results presented in Figures 2 and 3 only indicate the presence of the *Cc* and *R3c* phases in x = 0 and 3.5%, respectively, but do not necessarily suggest these two compositions are of single phase. Although recent studies indicate that the *Cc* symmetry seems to best fit $(Bi_{1/2}Na_{1/2})TiO_3$,[14–16] it has also been suggested that there are competing ferroelectric instabilities.[33,36] Should pure $(Bi_{1/2}Na_{1/2})TiO_3$ itself exhibits mixed phases, the same might be true for all the compositions with x <6%, and the sharp phase transition revealed by the electric-field-dependent strain measurements[32] only reflects an abrupt change in the volume fraction of the mixed phases. In this way, the phase boundary identified in this study separates the *Cc* phase dominant region ($x \leq 3\%$) from the *R3c* dominant region ($x \geq 4\%$). To include the existence of such a possibility, we mark the *Cc*/*R3c* "phase boundary" with dashed lines in Figure 4, in contrast to solid lines for other phase boundaries.

4. Conclusions

In conclusion, we proposed a more practical method to determine the oxygen octahedra tilting in perovskite ferroelectrics through selected area electron diffraction. The use of the domain wall edge-on conditions in our method allows the analysis of an ensemble of multiple domains, and significantly simplifies the specimen tilting in comparison with the commonly used method.[18,27] With this method, the phase relationship in $(1–x)(Bi_{1/2}Na_{1/2})TiO_3–xBaTiO_3$ with x <6% was clarified; a new phase boundary separating the *Cc* and *R3c* phases was revealed at x = 3–4%. In the E_{pol} versus x phase diagram for polycrystalline ceramics, this *Cc*/*R3c* phase boundary is curved, indicating that the previously unexplained electric-field-induced phase transition in the low-$BaTiO_3$-content compositions[32] is a *Cc*-to-*R3c* structural transition.

5. Experimental Section

Polycrystalline ceramic samples of $(Bi_{1/2}Na_{1/2})TiO_3–BaTiO_3$ were prepared via the solid-state reaction approach. Powders of Bi_2O_3 (≥99.9%), Na_2CO_3 (≥99.9%), $BaCO_3$ (≥99.99%) and TiO_2 (≥99.99%) were used as starting materials. Stoichiometric amount of powders were mixed and vibratory milled in ethanol with zirconia mill media for 7 h and then dried. The Na_2CO_3 powder was baked at 200 °C for 15 h and then weighed immediately to ensure stoichiometry. The mixture was calcined at 800 °C for 2 h and then vibratory milled for another 16 h. After drying, the powders were evenly mixed with binder (10 wt% polyvinyl alcohol solution) and then uniaxially pressed into pellets. Following binder burnout at 500 °C, sintering was carried out at 1150 °C to obtain dense ceramic pellets. In order to prevent the loss of Bi^{3+} and Na^+, the pellets were buried in a plenty amount of protective powder with the same composition during sintering. The relative density of the sintered pellets is higher than 97% as determined by the Archimedes' method. X-ray diffraction experiments confirmed pure perovskite phases in all ceramics.

As-sintered ceramic pellets were mechanically ground and polished down to about 150 μm thick for TEM specimen preparation. Disks with diameter of 3 mm were ultrasonically cut from the polished slices and the center portion was further thinned to around 5 μm by mechanical dimpling. The dimpled disks were annealed at 250 °C for 2 h, and then Ar-ion milled to electron transparency. TEM study was performed on a Phillips CM-30 microscope operated at 300 kV with a standard double-tilt specimen holder. Bright-field images and selected area electron diffraction patterns were recorded with a charge-coupled device camera.

Supporting Information

Supporting Information is available from the Wiley Online Library or from the author.

Acknowledgements

The National Science Foundation (NSF), through Grant DMR-1037898, supported this work. TEM experiments were performed at the U.S.-DOE Ames Laboratory.

Received: February 19, 2013
Revised: March 27, 2013
Published online: May 16, 2013

[1] M. Ahart, M. Somayazulu, R. E. Cohen, P. Ganesh, P. Dera, H.-K. Mao, R. J. Hemley, Y. Ren, P. Liermann, Z. Wu, *Nature* **2008**, *451*, 545.
[2] H. J. Lee, S. Zhang, J. Luo, F. Li, T. R. Shrout, *Adv. Funct. Mater.* **2010**, *20*, 3154.
[3] Z. Chen, Z. Luo, C. Huang, Y. Qi, P. Yang, L. You, C. Hu, T. Wu, J. Wang, C. Gao, T. Sritharan, L. Chen, *Adv. Funct. Mater.* **2011**, *21*, 133.
[4] J. Rödel, W. Jo, K. T. P. Seifert, E. M. Anton, T. Granzow, D. Damjanovic, *J. Am. Ceram. Soc.* **2009**, *92*, 1153.
[5] K. Wang, J.-F. Li, *Adv. Funct. Mater.* **2010**, *20*, 1924.
[6] D. Schütz, M. Deluca, W. Krauss, A. Feteira, T. Jackson, K. Reichmann, *Adv. Funct. Mater.* **2012**, *22*, 2285.
[7] R. Dittmer, W. Jo, J. Rödel, S. Kalinin, N. Balke, *Adv. Funct. Mater.* **2012**, *22*, 4208.
[8] W. Jo, J. E. Daniels, J. L. Jones, X. Tan, P. A. Thomas, D. Damjanovic, J. Rödel, *J. Appl. Phys.* **2011**, *109*, 014110.
[9] C. Ma, X. Tan, *Solid State Commun.* **2010**, *150*, 1497.
[10] C. Ma, X. Tan, E. Dul'kin, M. Roth, *J. Appl. Phys.* **2010**, *108*, 104105.
[11] C. Ma, X. Tan, *J. Am. Ceram. Soc.* **2011**, *94*, 4040.
[12] C. Ma, H. Z. Guo, S. P. Beckman, X. Tan, *Phys. Rev. Lett.* **2012**, *109*, 107602.
[13] G. O. Jones, P. A. Thomas, *Acta Cryst. B* **2002**, *58*, 168.
[14] S. Gorfman, P. A. Thomas, *J. Appl. Cryst.* **2010**, *43*, 1409.
[15] E. Aksel, J. S. Forrester, J. L. Jones, P. A. Thomas, K. Page, M. R. Suchomel, *Appl. Phys. Lett.* **2011**, *98*, 152901.
[16] I. Levin, I. M. Reaney, *Adv. Funct. Mater.* **2012**, *22*, 3445.
[17] M. Glazer, *Acta Cryst. A* **1975**, *31*, 756.
[18] D. I. Woodward, I. M. Reaney, *Acta Cryst. B* **2005**, *61*, 387.
[19] M. Reaney, E. L. Colla, N. Setter, *Jpn. J. Appl. Phys.* **1994**, *33*, 3984.
[20] Z. Xu, D. Viehland, P. Yang, D. A. Payne, *J. Appl. Phys.* **1993**, *74*, 3406.
[21] D. Viehland, Z. Xu, D. A. Payne, *J. Appl. Phys.* **1993**, *74*, 7454.
[22] D. Viehland, D. Forst, J. Li, *J. Appl. Phys.* **1994**, *75*, 4137.
[23] D. Viehland, *Phys. Rev. B* **1995**, *52*, 778.
[24] D. Viehland, M.-C. Kim, Z. Xu, J. Li, *Appl. Phys. Lett.* **1995**, *67*, 2471.
[25] X. Dai, Z. Xu, D. Viehland, *J. Appl. Phys.* **1996**, *79*, 1021.
[26] Q. Tan, Z. Xu, J. Li, D. Viehland, *J. Appl. Phys.* **1996**, *80*, 5866.
[27] D. I. Woodward, I. M. Reaney, R. E. Eitel, C. A. Randall, *J. Appl. Phys.* **2003**, *94*, 3313.
[28] Y. Sato, T. Hirayama, Y. Ikuhara, *Phys. Rev. Lett.* **2011**, *107*, 187601.
[29] J. Fu, R. Zuo, Z. Xu, *Appl. Phys. Lett.* **2011**, *99*, 062901.
[30] V. Dorcet, G. Trolliard, P. Boullay, *Chem. Mater.* **2008**, *20*, 5061.
[31] Y. Guo, Y. Liu, R. L. Withers, F. Brink, H. Chen, *Chem. Mater.* **2011**, *23*, 219.
[32] W. Jo, J. Rödel, *Appl. Phys. Lett.* **2011**, *99*, 042901.
[33] B. N. Rao, R. Ranjan, *Phys. Rev. B* **2012**, *86*, 134103.
[34] L. A. Schmitt, J. Kling, M. Hinterstein, M. Hoelzel, W. Jo, H.-J. Kleebe, H. Fuess, *J Mater. Sci.* **2011**, *46*, 4368.
[35] J. Yao, N. Monsegue, M. Murayama, W. Leng, W. T. Reynolds, Q. Zhang, H. Luo, J. Li, W. Ge, D. Viehland, *Appl. Phys. Lett.* **2012**, *100*, 012901.
[36] B. N. Rao, A. N. Fitch, R. Ranjan, *Phys. Rev. B* **2013**, *87*, 060102.